Solution Structure of the Ligand Binding Domain of the Fibroblast Growth Factor Receptor: Role of Heparin in the Activation of the Receptor[†,‡]

Kuo-Wei Hung,[§] Thallapuranam Krishnaswamy S. Kumar,[||] Karuppanan Muthusamy Kathir,[||] Ping Xu,[⊥] Feng Ni,[⊥] Hsiang-Hui Ji,[§] Mei-Chi Chen,[§] Chu-Chi Yang,[§] Fu-Pang Lin,[@] Ing-Ming Chiu,[#] and Chin Yu*[,§,||]

Department of Chemistry and Biochemistry, University of Arkansas, Fayetteville, Arkansas 72701, Department of Chemistry, National Tsing Hua University, Hsinchu 30043, Taiwan, Biotechnology Research Institute, National Research Council of Canada, 6100 Royalmount Avenue, Montreal, Quebec H4P 2R2, Canada, Department of Internal Medicine, The Ohio State University, 480 West 9th Avenue, Columbus, Ohio 43210-1228, and Graduate Institute of Marine Biotechnology, National Taiwan Ocean University, Taiwan

Received May 31, 2005; Revised Manuscript Received September 5, 2005

ABSTRACT: The three-dimensional solution structure of the ligand binding D2 domain of the fibroblast growth factor receptor (FGFR) is determined using multidimensional NMR techniques. The atomic root-mean-square distribution for the backbone atoms in the structured region is 0.64 Å. Secondary structural elements in the D2 domain include 11 β-strands arranged antiparallely into two layers of β-sheets. The structure of the D2 domain is characterized by the presence of a short flexible helix that protrudes out of the layers of β-sheets. Results of size exclusion chromatography and sedimentation velocity experiments show that the D2 domain exists in a monomeric state both in the presence and in the absence of bound sucrose octasulfate (SOS), a structural analogue of heparin. Comparison of the solution structure of the D2 domain with the crystal structure of the protein (D2 domain) in the FGF signaling complex reveals significant differences, suggesting that ligand (FGF) binding may induce significant conformational changes in the receptor. SOS binding sites in the D2 domain have been mapped on the basis of the $^{1}H-^{15}N$ chemical shift perturbation data. SOS binds to the positively charged residues located in β-strand III and the flexible helix. Isothermal titration calorimetry data indicate that the ligand (hFGF-1) binds strongly ($K_d \sim 10^{-9}$ M) to the D2 domain even in the absence of SOS. Binding of SOS to either the D2 domain or hFGF-1 does not seem to be the driving force for the formation of the D2−hFGF-1 binary complex. The function of SOS binding appears to stabilize the preformed D2−FGF binary complex.

Fibroblast growth factors (FGFs)[1] are present ubiquitously in all metazoan species ranging from nematodes such as *Caenorhabditis elegans* to mammals (*1*−*3*). FGFs play critical roles in key cellular processes, such as embryogenesis, angiogenesis, differentiation, tissue repair, and wound healing (*4*, *5*). In humans, the wide array of biological activities of FGFs is mediated by five types of FGF receptors [FGFRs (*6*−*8*)]. With the exception of FGF-1 which is a universal ligand and can bind to all the FGFRs, most other FGFs exhibit specific patterns of receptor binding (*9*). The prototypical FGFR consists of an extracellular domain, a single-pass transmembrane helix, and a cytoplasmic tyrosine kinase domain (Figure 1; *10*, *11*). FGF signaling is triggered by binding of the ligand (FGF) to the extracellular domain of the FGFR (*12*). The extracellular domain consists of three immunoglobulin-like (Ig-like) domains (termed as D1−D3) and an acid box (comprising a continuous stretch of four to eight acidic amino acids) placed between the D1 domain and the D2 domain (Figure 1; *13*, *14*).

Ligand (FGF)-induced dimerization of the receptor is a mandatory step in FGF-induced signaling (*15*). Binding of FGF to the extracellular domain of the FGFR leads to receptor dimerization and juxtaposition of the tyrosine residues in the cytoplasmic domain (*4*). Autophosphorylation of tyrosine residues in the receptor activates the downstream signaling process (*4*, *16*). Several models describing the architecture of the FGF signaling complex [consisting of the extracellular domains, heparin, and the ligand (FGF)] have been proposed (*17*). These models have been fiercely debated because the structural differences in the FGF signaling complex that has been described largely depended on the

[†] This study was supported in part by grants from the National Institutes of Health (NIH NCRR COBRE Grant 1 P20 RR15569), the Arkansas Biosciences Institute, and the National Science Council, Taiwan. The work at the Biotechnology Research Institute was supported by a Special International R&D program grant of the National Research Council of Canada, sponsored by the Government of Canada (NRCC Publication No. 47481).

[‡] The assigned chemical shifts for backbone and side chain resonances have been deposited in the BioMagResBank as entry 5943. The coordinates of the three-dimensional structure of the D2 domain have been deposited in the Protein Data Bank (entry 1WVZ).

* To whom all correspondence should be addressed. E-mail: cyu@uark.edu. Fax: (479) 575-4049. Telephone: (479) 575-5646.

[§] National Tsing Hua University.

[||] University of Arkansas.

[⊥] National Research Council of Canada.

[@] National Taiwan Ocean University.

[#] The Ohio State University.

[1] Abbreviations: FGF, fibroblast growth factor; FGFR, fibroblast growth factor receptor; SOS, sucrose octasulfate; NMR, nuclear magnetic resonance; ITC, isothermal calorimetry; ECD, extracellular ligand binding domain; TALOS, Torsion Angle Likelihood Obtained from Shift and Sequence Similarity.

10.1021/bi051030n CCC: $30.25
Published on Web 11/09/2005

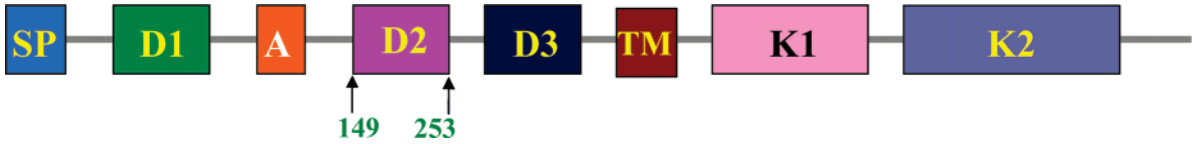

FIGURE 1: Schematic representation of the structural and functional domains of the fibroblast growth factors (FGFR2). SP, A, TM, K1, and K2 represent the signal peptide, acid box, transmembrane helix, kinase-1 domain, and kinase-2 domain, respectively.

method of crystallization (*14*, *15*, *18*−*21*). In addition, the unavailability of the three-dimensional solution structure of the free extracellular domain (in the absence of the ligand) has made it difficult to evaluate the physiological significance of the structure of the FGF signaling complex derived from crystal structures. Therefore, there is a growing need to characterize the three-dimensional structure of the ligand-free form of the extracellular ligand binding domain (ECD) of the FGFR. It is in this context, in this study, that we embarked on determination of the three-dimensional solution structure of the D2 domain of the ECD of the FGFR using multidimensional NMR spectroscopy.

The D2 and D3 domains of the ECD have been shown to be the minimal unit sufficient for ligand (FGF) binding (*13*, *14*). Truncated FGFRs devoid of the D1 domain exhibit ligand binding properties similar to those of the full-length receptor (*13*, *14*). The D3 domain dictates the specificity of ligand binding (*16*−*21*). The D2 domain contains the primary sites of binding for both the ligand and heparin (*16*−*21*). In the study presented here, we describe the three-dimensional solution structure of the D2 domain of FGFR2 using multidimensional NMR techniques. Significant differences could be discerned between the three-dimensional solution structure of the ligand-free form of the D2 domain and the structure of the D2 domain as present in the crystal structure of the FGF signaling complex (*19*, *20*). In addition, we have successfully mapped the heparin binding sites on the D2 domain using $^{1}H-^{15}N$ chemical shift perturbation data. Results obtained in this study appear to favor a 1:1:1 ternary D2−heparin−hFGF-1 complex in solution.

RESULTS AND DISCUSSION

Overexpression and Purification of the D2 Domain. The D2 domain construct used in this study is 104 amino acids long and spans residues 149−253 of the full-length FGFR2 receptor (*13*). Cloning, overexpression, and purification of the D2 domain of FGFR2 have been reported previously (*13*). The recombinant D2 domain was purified to homogeneity using nickel affinity and heparin−Sepharose chromatography. It has been shown that the D2 domain is an all-β-sheet protein and is capable of binding to both heparin and the ligand, hFGF-1.

Molecularity of the D2 Domain. The crystal structure of the FGF signaling complex supporting the Pelligrini model shows no direct FGFR−FGFR structural contacts (*17*). In marked contrast, the crystal structure of the FGF−FGFR−heparin/SOS ternary complex representing the Schlessinger model shows extensive receptor−receptor interactions mediated by the D2 domains of individual FGFR molecules (*14*). It is not clear if this observed disparity stems from the differences in the methods of crystallization (of the FGF signaling complex) employed by the two research groups. Direct structural contacts observed between the D2 domains of the individual receptor molecules in the Schlessinger model hint at the possibility of the isolated D2 domain to exist as a dimer in solution. In this context, we examined this possibility by investigating the molecularity of the isolated D2 domain in solution using size exclusion chromatography and analytical ultracentrifugation.

Sucrose octasulfate (SOS), a structural analogue of heparin, has been shown to mimic heparin by supporting the FGF-mediated cell proliferation activity in vitro (*22*). In addition, both heparin and SOS are shown to promote osteocalcin expression and promote complete closure of the cranial sutures (*15*). Crystal structure data show that SOS activates the receptor by binding to the heparin binding sites in both FGF and the D2 domain of the FGFR (*15*). It is in this context that we substituted SOS for heparin in all experiments described in this study. In addition, SOS was preferred over heparin because of problems encountered in preparation of homogeneous heparin samples (*22*−*25*). Size exclusion chromatography is a useful technique for monitoring the molecular association and dissociation and conformational changes in proteins on ligand binding. Under the experimental conditions that were used, the D2 domain in the absence of SOS elutes as a single peak with a retention time of ∼76 min (Figure 2). Extrapolation of the retention time of the D2 domain to a standard plot (of the logarithm of molecular masses of proteins vs the retention time of proteins) yields an approximate molecular mass (∼13.7 kDa) corresponding to the monomeric state of the protein. The molecular mass of the D2 domain only marginally increases (∼15.1 kDa) when it is complexed to SOS (∼1.2 kDa), suggesting that the isolated D2 domain exists as a monomer in solution both in the presence and in the absence of SOS (Figure 2).

The molecularity of the D2 domain in the presence and absence of SOS was also evaluated using sedimentation velocity experiments through analytical ultracentrifugation. Sedimentation velocity studies provide useful information about the molecular mass of macromolecules and help in the assessment of the presence of heterogeneous molecular states (of macromolecules) in equilibrium with each other (*26*). In this context, we performed the sedimentation velocity experiments on the D2 domain in the presence and absence of SOS. The D2 domain in its free state moves as a single boundary with a Svedberg constant ($S_{20,w}$) value of 1.46 ± 0.09 S (Figure 3A). The sedimentation coefficient of the D2 domain in the presence of an excess of SOS is estimated to be 1.49 ± 0.08 S (Figure 3B). Time-derivative analysis of the sedimentation velocity data reveals that the protein in its free and SOS-bound states comprises a single molecular species corresponding to molecular masses of ∼13.4 and ∼15.1 kDa, respectively. The amount of higher-molecular mass species formed in the presence and absence of SOS is insignificant. Therefore, the results of the sedimentation velocity experiments corroborate those obtained using size exclusion chromatography and unambiguously show that the

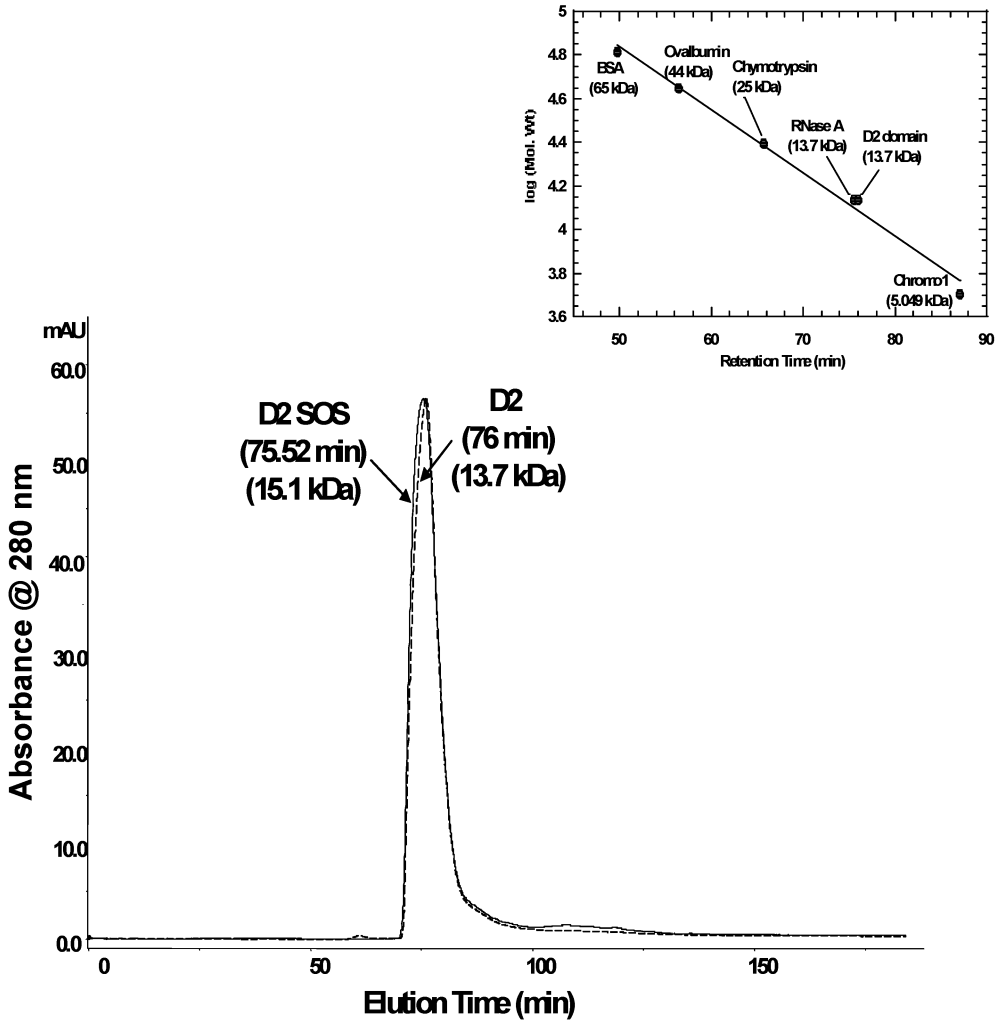

FIGURE 2: Size exclusion chromatographic profiles of the D2 domain in its free state (- - -) and the SOS-bound state (—). The inset shows the plot of the logarithm of the molecular masses of proteins vs the elution times of the proteins. The numbers included in parentheses represent the molecular masses of the proteins in kilodaltons. Elution of proteins was monitored by their absorbance at 280 nm. The flow rate of elution is 1 mL/min. The concentration of the proteins used in the experiment was ~1 mg/mL. Elution (at 298 K) was carried out using 10 mM phosphate buffer (pH 6.5) containing 50 mM NaCl and 50 mM ammonium sulfate.

D2 domain exists as a monomer both in its free form and in the SOS-bound form.

Resonance Assignments. Sequence specific assignments of the polypeptide backbone were made from $^{1}H-^{15}N$ HSQC, HNCO, HN(CO)CA, and CBCANH spectra. Ambiguities in the assignment were resolved by selective ^{15}N labeling of the protein. The $^{1}H-^{15}N$ HSQC spectrum of the D2 domain is well-dispersed, and almost all the resonances (excluding the six proline residues) have been assigned except for those of the backbone $^{1}H-^{15}N$ resonances of Met1, Asn2, Ala36, Lys54, Asn66, and Gln67 (Figure 4A). Side chain resonances were assigned from the combined information content of the ^{15}N-edited TOCSY-HQSC, ^{15}N-edited NOESY-HSQC, ^{13}C-edited NOESY-HSQC, HCCH-TOCSY, and HBHACONH spectra. The backbone dihedral angles were predicted using TALOS (*41*) and HNHA analysis.

Quality of the Three-Dimensional Structure of the D2 Domain. Structure models were first computed on the basis of distance geometry calculations and energy minimization with 1172 experimental and empirical NMR restraints, consisting of 975 NOE-derived approximate interproton distance constraints, 39 hydrogen bond-derived restraints, one disulfide restraint, and 157 dihedral angle constraints derived from measured scalar coupling constants as well as TALOS calculations (Table 1). A total of 20 structure models of the D2 domain thus obtained were further refined and validated by the incorporation of 37 $^{1}H-^{15}N$ long-range residual dipolar coupling (RDC) restraints. These RDC constraints were a conservative set selected from experimentally measured RDC values only for structurally defined residues identified on the basis of heteronuclear $^{1}H-^{15}N$ NOE data (Figure 4B) and in the set of 20 best conformers derived above. The NMR structure represented by the 20 best conformers has a good fit with the experimental data, as shown by very small residual constraint violations. There were no distance restraint and dihedral angle constraint violations greater than 0.2 Å and 1.4°, respectively. The rmsd value of the backbone atoms in residues 4−104 was estimated to be 0.64 Å (Figure 5). A summary of the structural statistics for the final 20 stimulated annealing structures of the D2 domain is provided in Table 1. The quality of the D2 domain NMR structure is also evident from the results of PROCHECK analysis, showing that most of the backbone torsion angles for non-glycine residues lie within the expected regions of the Ramachandran plot.

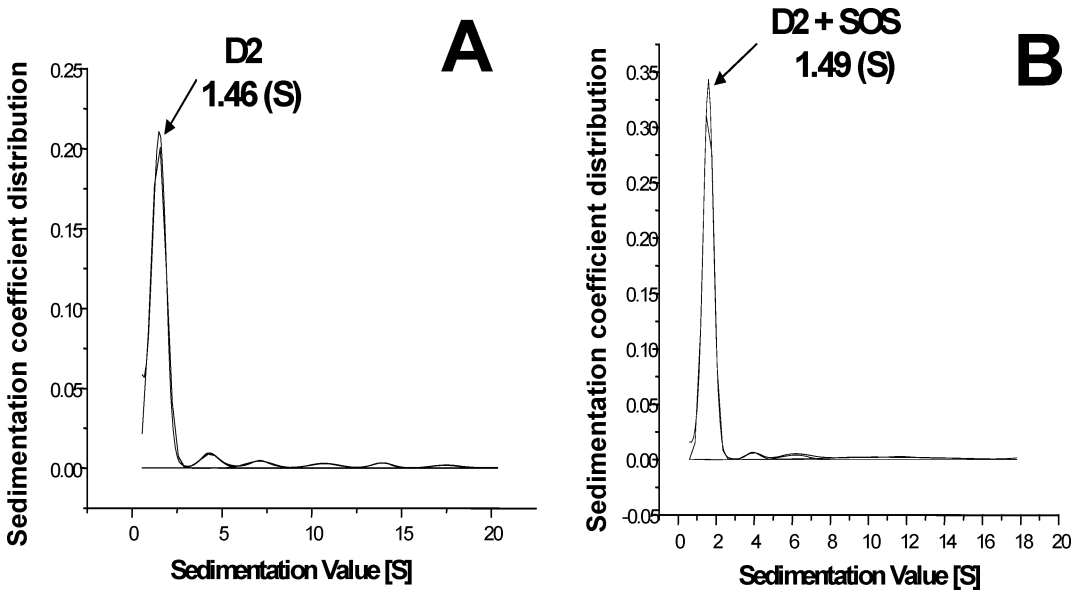

FIGURE 3: Sedimentation velocity fits (single-species fit) of the D2 domain in the absence (A) and presence (B) of SOS. The apparent sedimentation coefficient distribution [$c(s^*)$] analyses were based on the use of 100 scans recorded at 2 min intervals using interference optics with a rotor speed of 50 000 rpm at a protein concentration of 0.5 mg/mL. The sedimentation coefficient values for the D2 domain in the absence and presence of SOS are 1.46 and 1.49 S (shown in parentheses), respectively.

Description of the Structure. The D2 domain is a predominantly β-sheet protein with 11 β-strands arranged in an antiparallel fashion. The 11 β-strands [strand I (residues 10−12), strand II (residues 23−25), strand III (residues 29−33), strand IV (residues 36−38), strand V (residues 43−48), strand VI (residues 51−53), strand VII (residues 62−64), strand VIII (residues 70−74), strand IX (residues 83−90), strand X (residues 93−99), and strand XI (residues 103 and 104)] are uniformly distributed throughout the structure of the D2 domain (Figures 5 and 6A). Two distinct layers of β-sheets can be discerned in the structure of the D2 domain. One layer of the sheet is constituted by β-strands III, VII, and VIII, and the other is comprised of β-strands V, IX, and X. The two layers of β-sheets are linked through a disulfide bond between Cys34 and Cys86. The disulfide link is located in the core of hydrophobic residues and appears to confer conformational stability to the D2 domain. The structure of the D2 domain is also characterized by a short and flexible 3_{10}-helix (residues 15−17) located between β-strands I and II (Figure 6A). The 3_{10}-helix protrudes out of the two layers of β-sheet structures.

The local rmsd values of the 20 refined structures reveal some apparently highly flexible segments in the D2 domain consisting of residues 1−3, 54−61, and 66−68. The conserved signature "HAV" (-His-Ala-Val-) motif (residues 22−24 in the D2 domain) which is found in all cell adhesion molecules, including the FGFR, is a part of β-strand II (*27*). Ala23 which is part of the HAV motif is believed to interact with FGF-1 (*19*−*21*). The HAV motif in the D2 domain is solvent-exposed and thus poised for homophilic interactions with the ligand (hFGF-1). Similarly, the other putative ligand (FGF) binding sites are in a partially buried hydrophobic microenvironment formed by residues in the loop regions between β-strands VI and VII (residues 54−61) and VIII and IX (residues 75−82).

The solution structure of the D2 domain was further characterized by use of NMR relaxation experiments, in particular, by ^{1}H−^{15}N heteronuclear Overhauser effects (^{1}H−^{15}N NOEs). Figure 4B shows that many residues of the D2 domain exhibit ^{1}H−^{15}N NOE values for their amide ^{1}H and ^{15}N pairs of ∼0.8, which is characteristic of well-structured proteins. Therefore, the globular structure of D2 should start from residue 6 and end at residue 104, in excellent agreement with results from structural calculations (Figure 5). Specifically, high structure order is evident for the six β-strands making up the two core β-sheets, i.e., strands III (residues 29−33), VII (residues 62−64), and VIII (residues 70−74) for one β-sheet and strands V (residues 43−48), IX (residues 83−90), and X (residues 93−99) for the second β-sheet. Very interestingly, the loop residues (loop 4) between strands VII and VIII, i.e., residues 66−68, must be very flexible or conformationally heterogeneous, on the basis of a very negative ^{1}H−^{15}N NOE for residue 68 (Figure 4B) and missing HSQC peaks for residues 66 and 67. In contrast, large ^{1}H−^{15}N NOE values were also observed for residues within the four other loop regions, i.e., loop 1 connecting β-strands II and III, loop 2 connecting β-strands IV and V, loop 3 connecting β-strands VI and VII, and loop 5 connecting β-strands VIII and IX (Figure 4B). In other words, even many of the surface loops on the isolated D2 domain appear to have well-defined conformations, which is also shown by the calculated structures (Figure 5). The structural stability of these loops is strongly correlated with loops 3 (residues 54−61) and 5 (residues 75−82) being the predominant contact site for ligand (FGF) binding.

Comparison of the Solution Structure of the Isolated D2 Domain with the Crystal Structure of the D2 Domain in the FGF−FGFR Complex. The global fold of the solution structure of the D2 domain resembles that of the D2 domain in the crystal structure of the FGF−FGFR binary complex (*19*−*21*) (Figure 6A,B). The secondary structural elements in the solution and crystal structures are similar. However, superposition of the backbone of the X-ray and the NMR structures of the D2 domain yields a rmsd of 3.25 Å, suggesting significant differences in the spatial orientation of the backbone of the protein in the two structures. The

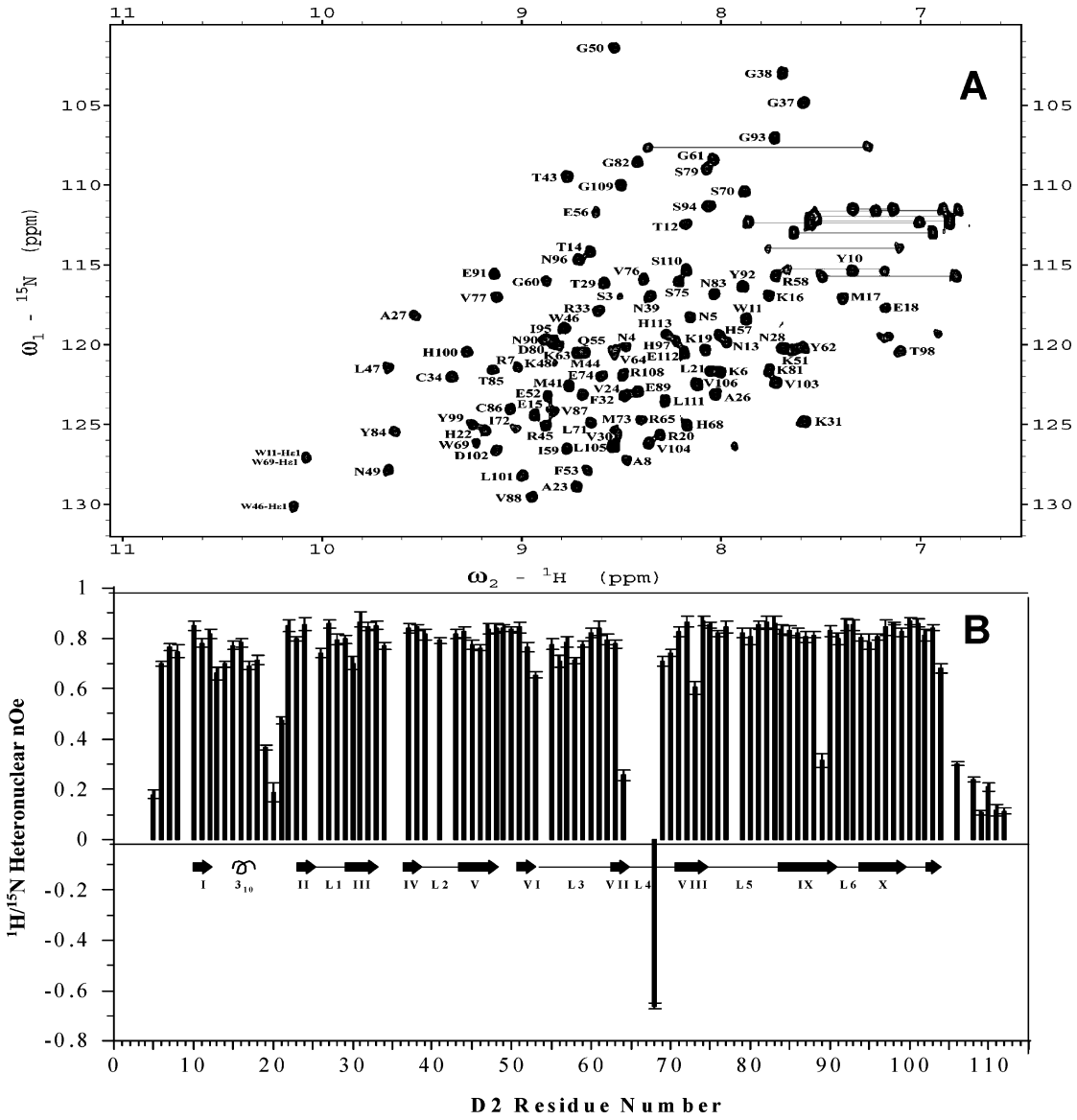

FIGURE 4: (A) ^{1}H−^{15}N HSQC spectrum of the D2 domain at 298 K in 10 mM phosphate buffer (pH 6.5) containing 50 mM NaCl and 50 mM ammonium sulfate. The spectrum is well-dispersed, suggesting that the D2 domain is mostly well structured in solution. (B) Plot of ^{1}H−^{15}N heteronuclear NOE values of the D2 domain acquired at 298 K. All the values were derived from data sets acquired at a ^{15}N resonance frequency of 81.068 MHz (800 MHz for protons). The block arrows indicate the locations of regular β-strands identified from calculated NMR structures (Figures 5 and 6A). The six surface loops, i.e., L1−L6, had the same locations as those of the X-ray structure of the D2 domain region (Figure 6B). A few ^{1}H−^{15}N NOE values are missing at the ends of some strand regions, which were confirmed (data not shown) to be of large values (>0.7) by use of the data set collected at the lower field of 500 MHz. These include residue 25 at the end of strand II and residue 36 at the beginning of strand IV. These discrepancies were largely caused by small differences in resonance overlaps for the HSQC spectra at different field strengths. Other missing NOE values were due to either resonance overlaps or missing HSQC peaks.

crystal and the solution structures differ prominently in the relative orientation of the two layers of β-sheets constituting the β-barrel architecture (Figure 6A,B). In the solution structure of the D2 domain, the layer of β-sheet comprising β-strands III, VII, and VIII subtends an angle of ~39° with the plane of the β-sheet consisting of β-strands V, IX, and X (Figure 6A). In the crystal structure, the corresponding layers of the β-sheet are tilted at an angle of ~17° with respect to each other (Figure 6B). The differences in the orientation of the two layers of β-sheets suggest that the D2 domain may undergo subtle conformational changes upon binding to the ligand (FGF). Structurally, such conformational changes can easily occur as the ligand (FGF) binding site resides mainly on the two surface loops (loops 3 and 5, Figure 4B) connecting the two layers of β-sheets (Figure 6A).

The topology of β-strand X appears to be significantly different in the solution and X-ray structures of the D2 domain (Figure 6A,B). β-Strand X in the crystal structure is long and rigid and extends to the C-terminal end of the molecule (residues 93−104). Interestingly, in the solution structure, β-strand X is interrupted by the presence of a short loop or at least an irregular strand consisting of residues 100−102. As a consequence, a short β-strand XI pairs with a shortened β-strand II. In other words, β-strand II in the crystal structure is longer (residues 21−25) than that observed in the solution structure (residues 23−25) of the D2 domain (Figure 6A,B). Critical analysis of the D2 domain

Table 1: Structural Statistics of the D2 Domain[a]

no. of NMR constraints	
distance constraints	
intraresidue	349
sequential ($\|i - j\| = 1$)	273
medium-range ($\|i - j\| = 4$)	72
long-range ($\|i - j\| = 5$)	281
hydrogen bond constraints	39
dihedral angle constraints	157
residual dipolar constraints	37
violation statistics (20 structures)	
maximum distance violation (Å)	0.2
maximum dihedral angle violation (deg)	1.4
X-PLOR energy (kcal/mol)	
E_{total}	149.74 ± 16.93
E_{bond}	6.13 ± 1.03
E_{angle}	67.82 ± 7.34
$E_{improper}$	14.28 ± 3.02
E_{NOE}	20.60 ± 9.62
E_{vdw}	17.55 ± 4.13
rmsd from ideal geometry	
bond lengths (Å)	0.002 ± 0.000
bond angles (deg)	0.357 ± 0.020
improper angles (deg)	0.296 ± 0.032
rmsd from experimental constraints	
distances (Å)	0.023 ± 0.011
dihedral angles (deg)	1.029 ± 0.207
rmsd for the structured region[a] (Å) (backbone)	0.452
rmsd for the structured region[a] (Å) (heavy atoms)	1.361
rmsd for the whole protein[b] (Å) (backbone)	0.640
rmsd for the whole protein[b] (Å) (heavy atoms)	1.639
PROCHECK parameter (%)	
most favored region	79.5
additionally allowed region	16.9
generously allowed region	2.8
disallowed region	0.8

[a] Residues in the structured regions: 10−12, 15−17, 23−25, 29−33, 36−38, 43−48, 51−53, 62−64, 70−74, 83−90, 93−99, and 102−104. [b] Residues 4−104.

in the crystal structures of the FGF−FGFR complex reveals that His22, Ala23, Leu101, and Asp102 are involved in interactions with hFGF-1 (*15*, *18*). Interestingly, His22, Leu101, and Asp102 are all located near the loop regions adjoining β-strands II and XI (Figure 6A,B). Ala23 is located at the fringe of β-strand II. Those residues located in the loop regions at one end of the D2 domain structure appear to provide an interface for extensive interactions with the FGF molecule. Location of these residues in the mostly irregularly structured regions of the isolated D2 domain may strengthen the binding of FGF to the D2 domain. Such enhanced binding may come from locking together the loop regions of D2 with FGF residues, resulting in the extension of β-strands II and X (as observed in the crystal structures of the D2 domain in the FGF−FGFR complex). Therefore, the solution structure of the D2 domain provides useful insights into the conformational elements important for recognition and binding of the ligand (FGF).

Mapping SOS Binding Sites in the D2 Domain. It is important to understand if the heparin (SOS) binding site(s) in the solution structure of the D2 domain is similar to the ones observed in the D2 domain portion of the crystal structure of the FGF−FGFR complex. In this regard, the ^{1}H−^{15}N HSQC spectrum serves as a fingerprint of the protein conformation, and each cross-peak in the spectrum represents the microenvironment of an amino acid residue in the protein (*28*). Therefore, on the basis of the chemical shift perturbation (that occurs upon addition of a ligand) observed in the ^{1}H−^{15}N HSQC spectrum, the binding site(s) of the ligand on the target protein can be conveniently mapped (*28*). Most of the cross-peaks in the ^{1}H−^{15}N HSQC spectrum remain unperturbed upon titration of the D2 domain with sucrose octasulfate (SOS, Figure 7A,B). However, ^{1}H−^{15}N cross-peaks of residues located at the flexible 3_{10}-helix and β-strand III, including Glu15, Lys16, Met17, Lys31, Phe32, and Ser70, exhibit significant perturbation upon addition of SOS, suggesting that these residues constitute or are located in the proximity of the SOS binding site in the protein (Figure 7C). Interestingly, the heparin (or SOS) binding sites in the solution structure of the D2 domain and the D2 domain portion of the crystal structures of the FGF−FGFR−heparin ternary complex are quite similar (*20*, *21*). The crystal structure of the D2 or D3 domain−SOS−hFGF-1 ternary complex also shows that heparin or SOS binds to the positively charged lysine residues (Lys16, Lys19, Lys28, Lys31, and Lys33) in the D2 domain (*15*).

^{1}H−^{15}N chemical shift perturbation data not only provide information about the ligand−protein interaction sites but also could provide useful information about the stoichiometry of these interactions (*28*). The stoichiometry of the SOS−D2 domain interaction was monitored on the basis of titration curves, individual residues in the D2 domain, generated on the basis of weighted average ^{1}H−^{15}N chemical shift changes. Titration curves of all residues monitored tend to saturate at an ∼1:1 D2 domain SOS ratio (Figure 7D).

Role of Binding of Heparin or SOS to the D2 Domain. There are conflicting views on the roles of proteoglycans such as heparin in FGF signaling (*22*, *23*, *25*, *29*). Heparin is believed to play a critical role in the recognition and binding of FGF to its cell surface receptor (*22*, *23*). It is believed that heparin not only increases the ligand (FGF)−receptor (FGFR) affinity but also promotes dimerization of the FGF−FGFR half-complexes by stabilization of protein−protein interactions between the two half-complexes (*22*). Interestingly, several studies suggest that heparin is involved in the dimerization of FGF, and the heparin-induced dimerization of the ligand (FGF) is believed to be the rate-limiting step in the activation of the cell surface receptor (*11*, *21*). In contrast, several other reports indicate that the function of heparin is limited to recruitment of the sparsely populated FGF molecules which consequently increase the probability of association of FGF with its receptor. There are numerous studies which suggest that there is no mandatory requirement of heparin for the binding and activation of the FGF receptor (*29*). Heparin is believed to merely stabilize FGF and the FGF−FGFR complex against the action of proteolytic enzymes (*25*). Roghani et al. demonstrated that the FGFR expressed in Chinese hamster ovary deficient in heparin sulfate synthesis can bind to human FGF-2 (*31*). Similarly, Delehedde et al. (*32*), using chlorate-treated rat mammary fibroblasts, showed that FGF-2 can bind to the FGFR and trigger transient early phosphorylation of p42/42^{MAPK} and p90^{RSK}. We recently demonstrated that newt FGF-1 in the presence of SOS exists in a monomeric state and exhibits cell proliferation activity similar to that observed in the presence of heparin (*25*). Similarly, Burgess and co-workers (*33*) and Byrch et al. (*34*) generated several mutants of FGF-1 which exhibit heparin-independent cell proliferation activity.

In an attempt to shed further light on the role(s) of heparin in FGF signaling, we studied the individual binding affinities

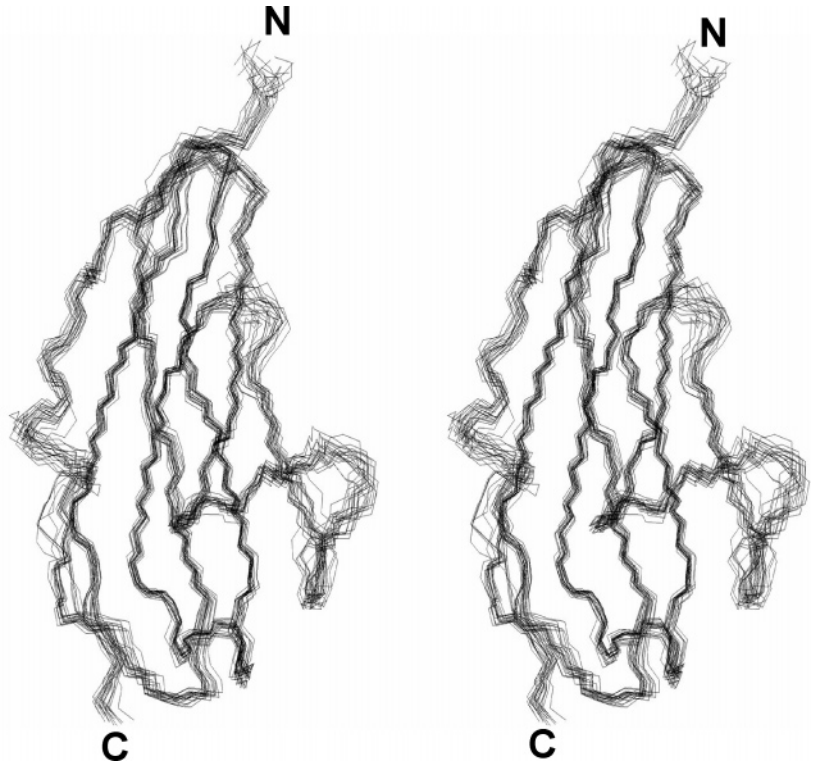

FIGURE 5: Stereoview of the three-dimensional structures of the D2 domain of the FGFR. The ensembles of 20 structures were calculated using NOE constraints. The D2 domain consists of 11 β-strands arranged in two layers of β-sheets. The labels N and C show the locations of the N- and C-terminal ends of the protein, respectively.

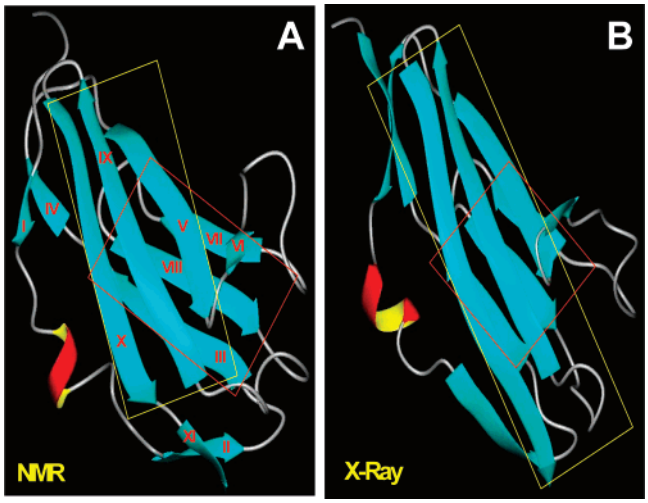

FIGURE 6: Comparison of the backbone folding of the D2 domain in solution (A) and in the crystal structure (B) of the FGF−FGFR complex. The solution and X-ray structures differ significantly in the orientation of the two layers of β-sheets. In addition, β-strands II and X are longer in the crystal structure than those observed in the solution structure of the D2 domain. The number of each β-strand (cyan) is indicated in Roman numerals. The short flexible helix is colored red. The two colored boxes outline the two layers of β-sheets in the NMR and X-ray structure of the D2 domain.

of SOS for hFGF-1, the D2 domain, and the D2−hFGF-1 binary complex using isothermal titration calorimetry (ITC). The D2 domain is an ideal molecule for investigating the role(s) of heparin in the formation of the FGF signaling complex because available crystal structure data suggest that the heparin contact sites on the FGFR are mostly located in the D2 domain (*18*−*21*). In addition, residues in the D2 domain are shown to extensively interact with the ligand (FGF-1; *18*, *21*). Isothermal titration calorimetry (ITC) is a useful technique for measuring the binding affinity of a protein for its ligand (*35*, *36*). ITC measurements also facilitate the estimation of the binding stoichiometry of protein−ligand interactions (*35*). Binding isotherms representing the interaction of SOS individually with FGF-1, the D2 domain, and the D2−FGF-1 binary complex are exothermic and proceed with the evolution of heat (Figure 8). Interaction of SOS with its protein partners (FGF-1 and D2 domain) is characterized by a large negative enthalpy change indicating that these interactions are predominantly mediated through charge interactions (Table 2). The binding isotherms representing binding of SOS to its protein partners are very sensitive to the buffer conditions used because of the dominance of charge−charge interactions in these reactions (*13*). The binding curve characterizing SOS−FGF-1 interaction is sigmoidal and fits best to a single-binding site model, yielding a binding constant (K_d) of 59 μM (Figure 8A and Table 2). The binding affinity of SOS for the D2 domain ($K_d \sim 27$ μM; Table 2) is on the same order of magnitude as that observed for SOS−hFGF-1 interaction. The SOS−D2 binding curve can be best fit to one high-affinity binding reaction with ~1:1 SOS:D2 domain stoichiometry (Figure 8B). The change in enthalpy of the interaction between SOS and D2 domain is negative (Table 2; $\Delta H \sim -12$ kcal/mol), suggesting that charge−charge interactions also play a dominant role in the SOS−D2 domain binding. Interestingly, the binding isotherm representing D2−SOS interaction reveals that the binding affinity between D2 and SOS decreases more than 100-fold when the NaCl concentration is increased from 100 to 300 mM (data not shown). These results suggest that charge interactions play a dominant role in the D2−SOS interaction. This conclusion is consistent

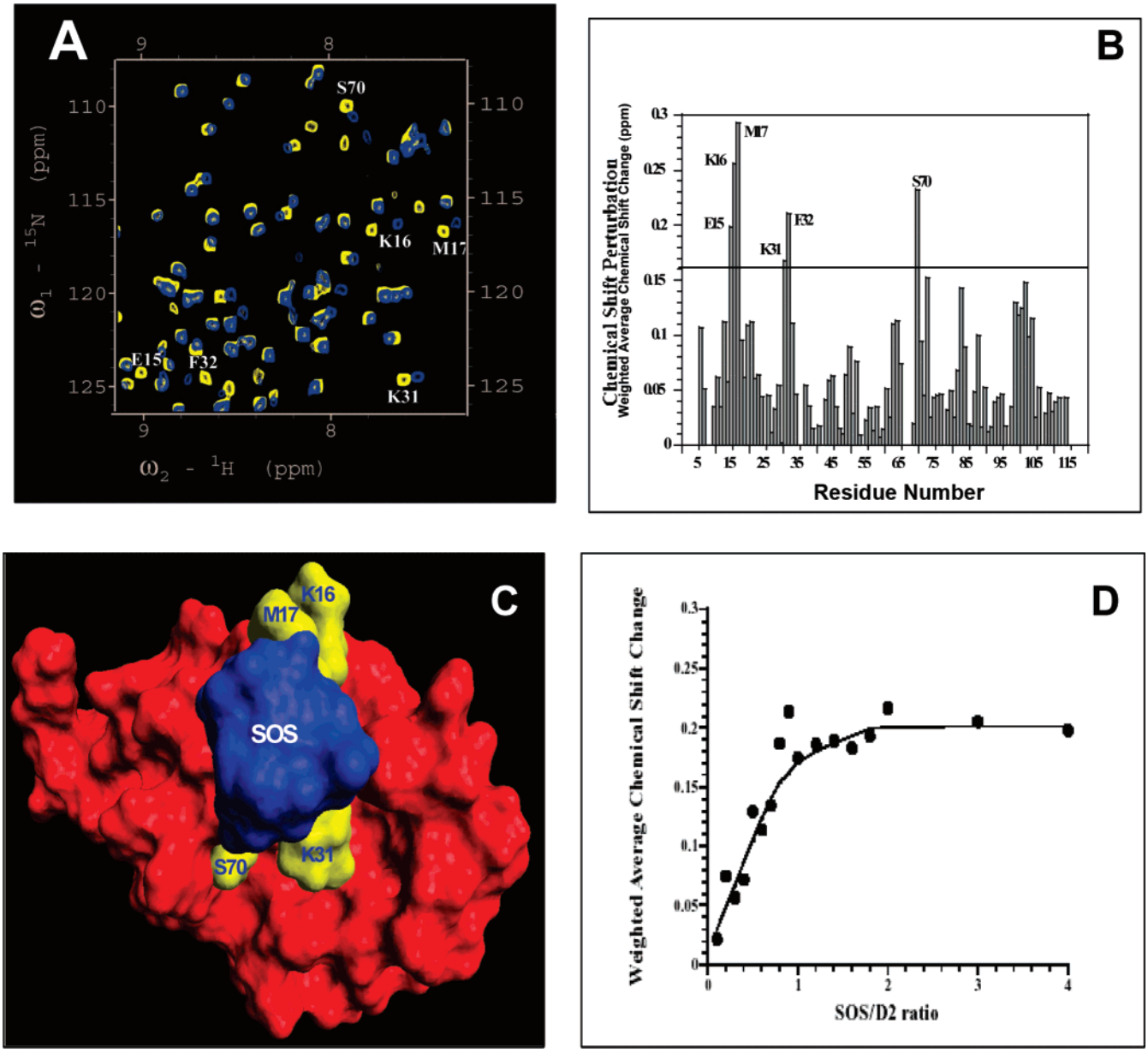

FIGURE 7: (A) Portion of the ^{1}H−^{15}N HSQC spectra of the D2 domain in the presence (blue) and absence (yellow) of SOS. Cross-peaks of residues involved in SOS binding show significant chemical shift perturbations. (B) Weighted chemical shift perturbation plot of the D2 domain in the presence of SOS. Glu15, Lys16, Met17, Lys31, Phe32, and Ser70 appear to be located in the proximity of the SOS binding site. (C) Model of the complex structure of the D2 domain (red) bound to SOS (blue). The residues that exhibit significant chemical shift perturbation are colored yellow. SOS binding sites in the D2 domain and hFGF-1 come together to form a continuous SOS binding groove (colored blue). (D) Titration curve of Glu15 as monitored by the weighted average shifts of the ^{1}H−^{15}N cross-peaks. The titration curve saturates at a SOS:D2 domain ratio of 1:1, suggesting that the D2 domain:SOS binding stoichiometry is 1:1.

with the ^{1}H−^{15}N chemical shift perturbation data which show that SOS binds to positively charged residues in the D2 domain. Interestingly, the binding constant characterizing the SOS−D2 domain interaction is in the same range as that reported for heparin binding to the entire receptor molecule, implying that the heparin and/or SOS binding sites on the FGFR are largely contributed by the D2 domain (*6*, *37*).

The binding curve representing interaction of the D2 domain with hFGF-1 is hyperbolic, suggesting that the interaction between these proteins is strong and highly cooperative (Figure 8C). The binding isotherm fits best to a one-site binding model with 1:1 hFGF:D2 domain stoichiometry. hFGF-1 and the D2 domain bind with very high affinity ($K_d \sim 65$ nM; Table 2). Binding reaction at the high-affinity site proceeds with a large negative enthalpy change ($\Delta H \sim -3$ kcal/mol; Table 2), suggesting that interaction(s) between the D2 domain and hFGF-1 is governed by charge−charge interactions. The binding curve representing the titration of the D2 domain and hFGF-1 (in the presence of SOS) is also hyperbolic and fits best to a one-site binding model (Figure 8D). The binding stoichiometry between hFGF-1 and the D2 domain does not change (∼1:1) upon binding to SOS. However, in the presence of SOS, the binding constant of the D2 domain and hFGF-1 shows a 1000-fold increase, suggesting that SOS stabilizes the preformed hFGF-1−D2 domain binary complex (Table 2).

Model of the Structural Events Leading to the Formation of the D2 Domain−SOS−hFGF-1 Ternary Complex. On the basis of the results obtained in this study, we propose a model of the structural events involved in the formation of the D2

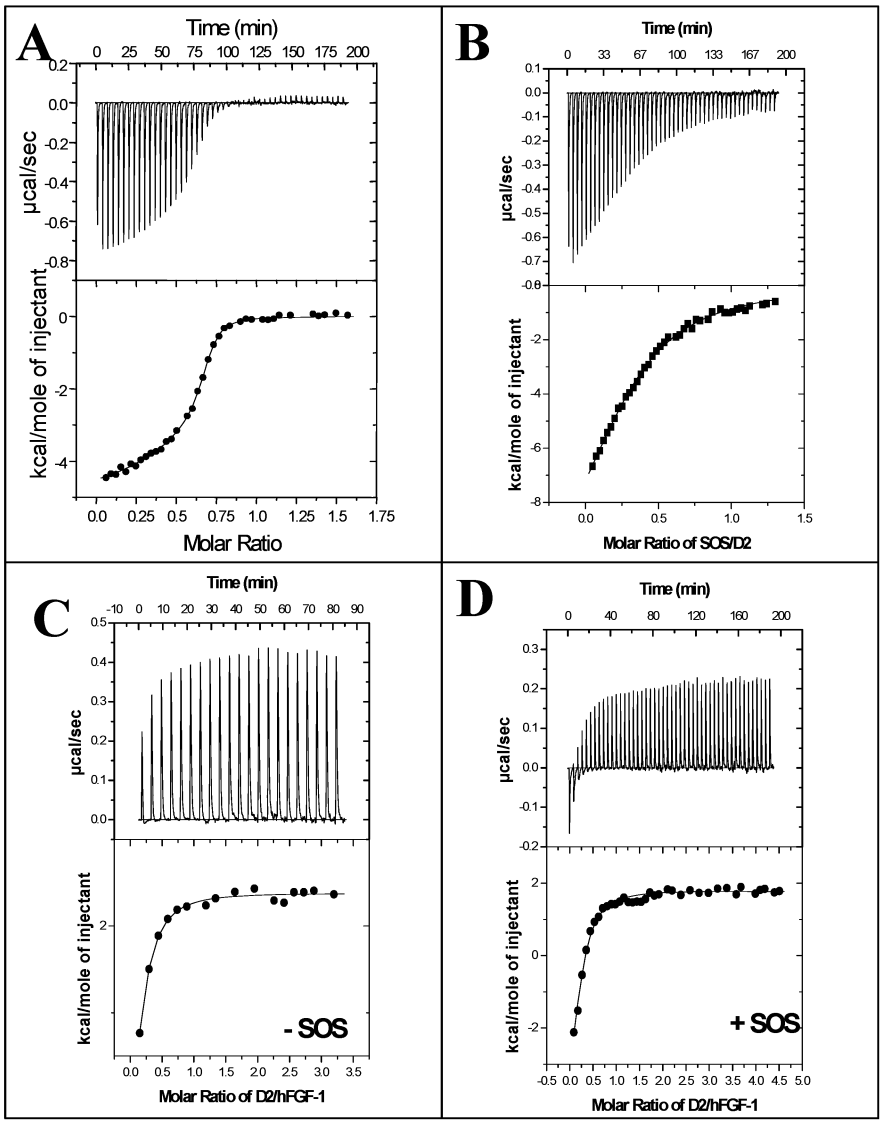

FIGURE 8: Binding isotherm for the titration of SOS with hFGF-1 (A), SOS with the D2 domain (B), and hFGF-1 with the D2 domain without (C) and with (D) SOS. The top panels show the raw data for the titration. The bottom panels show the integrated data obtained from the raw data, after subtraction of the heat of dilution. The solid lines in the bottom panels represent the best-fit curves to the data, using the one-independent site model from Microcal Origin. The binding parameters estimated from these experiments are given in Table 2.

Table 2: Binding Parameters Derived from ITC Experiments

experiment no.	protein	ligand	K_d[a]	ΔH[b] (kcal/mol)
1	hFGF	SOS	$59 \pm 0.01\ \mu$M	-7.4 ± 0.18
2	D2	SOS	$27 \pm 0.8\ \mu$M	-12 ± 0.3
3	D2	hFGF	65 ± 0.4 nM	-3 ± 0.1
4	D2	hFGF−SOS	20 ± 0.2 pM	-6 ± 0.08

[a] K_d represents the binding constant for the binding site. [b] ΔH represents the change in enthalpy.

domain−SOS−hFGF-1 complex. In this model, interaction between the D2 domain and hFGF-1 would be the first molecular event in the activation of the receptor (Figure 9). ITC data show that the D2 domain and hFGF-1 bind with high affinity in a 1:1 binding stoichiometry. Results of the size exclusion chromatography and sedimentation velocity experiments show that both FGF-1 and the D2 domain remain in their monomeric states even upon binding to SOS. It appears that the SOS binding sites in both the D2 domain and FGF-1 may come together to form a continuous "SOS binding groove" in the D2 domain−hFGF-1 binary complex (Figure 9). A single molecule of SOS may bind in the SOS binding groove and interacts with residues in both the D2 domain and hFGF-1 (Figure 9). Furthermore, the D2 domain−SOS−hFGF-1 ternary complex is very stable under solution conditions. Results of this study therefore clearly suggest that SOS per se does not promote formation of the D2−hFGF-1 binary complex but merely stabilizes the preformed receptor−ligand complex.

The D2 domain is the basic functional unit of the FGFR as it provides the interface for binding to both the ligand (FGF) and heparin or SOS. Therefore, the three-dimensional solution structure of the D2 domain described in this study provides an avenue for further investigating the interplay of the molecular forces that govern the specificity of formation of the FGF signaling complex under physiological conditions. In addition, the availability of the solution structure of the D2 domain is expected to provide the necessary impetus for the rational design of potent therapeutic principles against FGF-mediated pathogenesis.

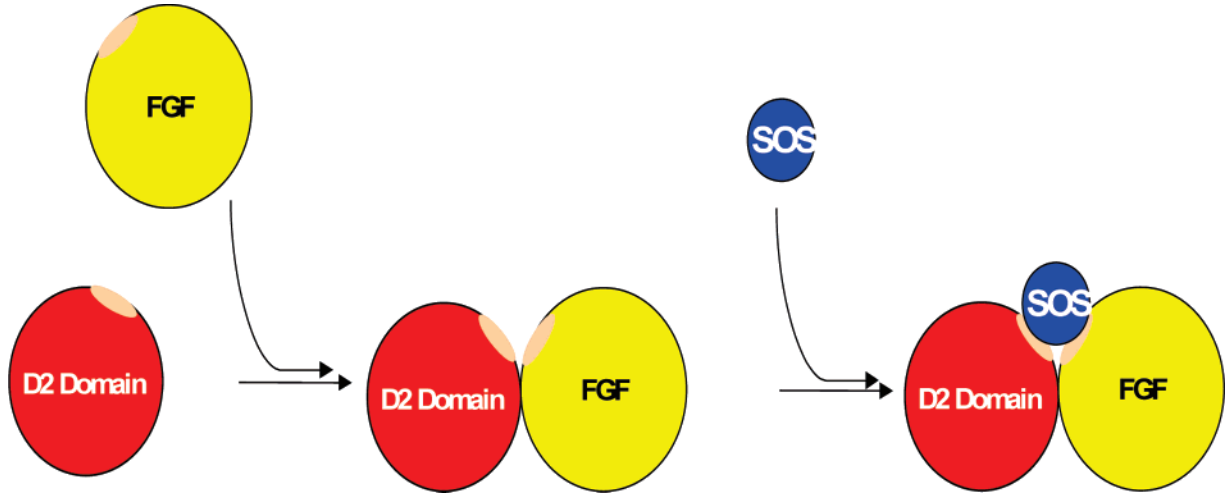

FIGURE 9: Schematic model representing the structural events in the formation of the D2 domain−SOS−FGF-1 ternary complex. The D2 domain (red) and hFGF-1 (yellow) can bind independently without the involvement of SOS. Upon interaction, the SOS binding sites in both the D2 domain and hFGF-1 (pink) come together to form a continuous SOS binding groove in the receptor domain−ligand binary complex. A single molecule of SOS (blue) binds to the SOS binding groove and has structural contacts with residues in both the D2 domain and hFGF-1. The 1:1:1 D2 domain−SOS−hFGF-1 ternary complex is very stable in solution, as shown by this study.

EXPERIMENTAL PROCEDURES

Materials. Taq DNA polymerase, *Nde*I, and *Xho*I enzymes were purchased from Promega. *Escherichia coli* [BL21-(DE3)pLysS] and pET20b(+) were purchased from Novagen. Sucrose octasulfate (SOS) and heparin−Sepharose were obtained from Toronto Research Chemicals (Toronto, ON) and Amersham Biosciences, respectively. Labeled $^{15}NH_4$-Cl, [^{13}C]glucose, and D_2O were purchased from Cambridge Isotope Laboratories. Acetonitrile, urea, and imidazole were obtained from Sigma Chemical Co. All other chemicals used in this study were of high-quality analytical grade.

Expression and Purification of the D2 Domain. The expression and purification of the D2 domain were carried out using the methods reported by Hung et al. (*13*). Isotope-enriched (^{15}N and ^{13}C) samples of the D2 domain were prepared using the procedure of Chi et al. (*38*).

Isothermal Titration Calorimetry (ITC) Measurements. Titration calorimetry measurements were performed with a Microcal (Northampton, MA) VP titration calorimeter. Samples were centrifuged prior to the titration and were examined for precipitates, if any, after the titration. A typical titration consisted of injecting 5−10 μL aliquots of 1 mM ligand (FGF) solutions into a 0.025−0.04 mM D2 domain solution after every 4 min to ensure that the titration peak returned to the baseline prior to the next injection. To measure the heats of dilutions, ligand solutions (at the same concentration that was used in the test titrations) were titrated against the reaction buffer [20 mM phosphate buffer (pH 6.5) containing 50 mM NaCl and 50 mM ammonium sulfate].

Size Exclusion Chromatography. Gel filtration experiments were performed at room temperature on a Superdex-75 column (using an AKTA FPLC device purchased from Amersham Biosciences). The protein sample was incubated with sucrose octasulfate (SOS) in 10 mM phosphate buffer containing 100 mM sodium chloride and 100 mM ammonium sulfate for 3 h at 277 K before being loaded onto the Superdex-75 column. All the protein samples were normalized to 0.5 absorbance unit before being loaded onto the column. Then, 10 mM phosphate buffer (pH 6.5) containing 50 mM NaCl and 50 mM ammonium sulfate was used as the eluent. The flow rate of the eluent was set at 1 mL/min. Protein peaks were detected by their 280 nm absorbance. Under the experimental conditions that were used, no shrinkage of the resin was observed. A standard plot of the logarithm of the molecular mass of proteins versus the elution time of proteins was constructed using proteins in the molecular mass range of 6−66 kDa. Experimental conditions used for the elution of standard proteins were the same as those for the D2 domain.

Sedimentation Velocity Experiments. Sedimentation velocity experiments were performed on a Beckman-Coulter Optima XL-A analytical ultracentrifuge equipped with An-60 Ti analytical rotor and standard double-sector cells. Sedimentation velocity experiments with the D2 domain of the FGFR (in the presence and absence of SOS) were performed under identical conditions. Sedimentation velocity experiments were performed at 277 K and 50 000 rpm for 20 h. The Svedberg constant ($S_{20,w}$) values were estimated using standard methods. The sedimentation boundary movement was traced by the absorbance of the protein using a built-in UV detector. The protein:SOS ratio used in these experiments was 1:1. The concentration of the protein (D2 domain) was 1.5 mg/mL.

NMR Experiments. NMR experiments were performed on Bruker Avance-800 and DMX-700 MHz spectrometers. NMR data for the D2 domain were acquired at a protein concentration of 1.5 mM in 20 mM phosphate buffer [in 90% H_2O and 10% D_2O (pH 6. 5)] containing 50 mM NaCl and 50 mM ammonium sulfate. All triple-resonance experiments were carried out at 298 K to accomplish complete assignment of ^{1}H, ^{13}C, and ^{15}N resonances in the protein. Homonuclear two-dimensional experiments [TOCSY (mixing time of 75 ms) and NOESY (mixing time of 200 ms)] were acquired for samples of the unlabeled D2 domain of the FGFR. All heteronuclear two- and three-dimensional experiments were performed with a sample of uniformly ^{13}C- and ^{15}N-labeled protein. The three-dimensional NMR experiments performed on the D2 domain include HNHA, HNCA, HNCO, HN(CA)-CO, CBCA(CO)NH, CC(CO)NH, HCCH-TOCSY, ^{13}C HSQC-TOCSY, ^{15}N HSQC-TOCSY, ^{13}C HSQC-NOESY,

and ^{15}N HSQC-NOESY (*39*, *40*). Backbone torsional angle restraints were derived from ^{3}J coupling constants measured by three-dimensional HNHA in combination with TALOS (Torsion Angle Likelihood Obtained from Shift and Sequence Similarity) calculations (*41*) and the pattern of medium-range NOE. DSS was used as an internal standard for calibration of the proton resonances. The slowly exchanging amide protons were identified by recording two-dimensional ^{15}N−^{1}H HSQC experiments 1 day and 5 days after the protein was dissolved in a D_2O solution. This information combined with the strong HN−Hα connectivities within and between β-stands enabled the identification of the β-strands and of the hydrogen bonds between the β-strands. For ^{15}N and ^{13}C chemical shift calibration, we followed the IUPAC procedure defined by Markley et al. (*42*). The water resonance was suppressed by applying a WATERGATE sequence or by presaturation. The three-dimensional spectra were processed and analyzed using XWINNMR and Sparky (*43*).

The residual dipolar coupling constants (RDCs) were measured using semi-TROSY spectra acquired at 298 K on a Bruker Avance-800-NMR spectrometer with the ^{1}H and ^{15}N carrier frequencies set to 4.7 and 119.35 ppm, respectively (*47*). A reference spectrum of ^{15}N-labeled D2 alone was acquired prior to the addition of 20 μL of a 50 mg/mL solution of *Pseudomonas aeruginosa* Pf1 phage (profos AG). The Pf1 phage was prepared by dialyzing overnight against the same sample buffer. The semi-TROSY spectrum in the presence of phages was recorded using the same experimental conditions and NMR parameters. Heteronuclear steady-state NOE values were measured at 298 K on both Avance-500 and 800 NMR spectrometers using a procedure described previously (*48*). Saturation of 3 s on the NH proton resonances and a recycle delay of 6 s were used in all experiments. The data set acquired at the higher field (i.e., 800 MHz for the ^{1}H frequency) was used for the analysis, which provided the needed spectral resolution for residues with very close resonance frequencies for their ^{1}H and ^{15}N nuclei. Heteronuclear NOEs were also examined using data sets acquired at the lower spectrometer field (i.e., 50.5777 MHz for the ^{15}N resonance frequency).

Structure Calculation. Families of structures were calculated by a simulated annealing (SA) approach followed by a refinement procedure using CNS-ARIA version 3.1 (*44*). Slightly modified slow-cooling standard simulated annealing protocols were used for the calculations. Structure refinement was carried out against the standard covalent geometry restraints. Constraints resulting from NOE intensities, coupling constants, and hydrogen bonds were introduced into the simulated annealing approach in a step-by-step manner. Sequential, medium-range, and long-range NOEs defining the β-sheet regions and coupling constants were used for structure calculations. All the remaining NOEs and hydrogen bonds were subsequently introduced in consecutive steps. The force field parameters used in the water refinement were those from PARALLHGS.2. The force constants used for the bond lengths, bond angles, ω angles, and improper dihedral angles in the cooling stage are 130 kcal mol^{-1} Å^{-2} and 80, 18, and 180 kcal mol^{-1} rad^{-2}, respectively. The quality of the constraints was checked by analyzing the violations of the calculated conformers. The NOE cross-peaks corresponding to constraints that were consistently violated in a significant number of structures were checked for possible overlap, and the corresponding restraints were consequently modified. A total of 20 structures with lowest combined distance and dihedral angle violations were sorted by restraint violation energy and selected for analysis. Backbone analysis were performed using PROCHECK (*45*).

The final NOE-based structures of the D2 domain were further refined by inclusion of a subset of experimental RDC-based constraints. The magnitude of the dipolar coupling tensor (D_a^{NH}) and the rhombicity factor (R) were estimated to be 11.0 and 0.6, respectively, from the histogram of the experimentally determined residual dipolar coupling constants. Only 37 dipolar coupling constants were selected for the residues located in the structurally well-defined regions, on the basis of both high heteronuclear NOE values and low rmsds of the structure ensembles before further refinement.

ACKNOWLEDGMENT

We thank Dmitri Tolkatchev, Kenji Tonan, Ping Wang, and Andy Ng for helpful advice and discussions.

REFERENCES

1. Lindner, V., and Maciag, T. (2001) The putative convergent and divergent natures of angiogenesis and arteriogenesis, *Circ. Res. 89*, 747−749.
2. Angulo, J., Ojeda, R., de Paz, J. L., Lucas, R., Nieto, P. M., Lozano, R. M., Redondo-Horcajo, M., Gimenez-Gallego, G., and Martin-Lomas, M. (2004) The activation of fibroblast growth factors (FGFs) by glycosaminoglycans: Influence of the sulfation pattern on the biological activity of FGF-1, *ChemBioChem 5*, 55−61.
3. Itoh, N., and Ornitz, D. M. (2004) Evolution of the Fgf and Fgfr gene families, *Trends Genet. 20*, 563−569.
4. Schlessinger, J. (2004) Common and distinct elements in cellular signaling via EGF and FGF receptors, *Science 306*, 1506−1507.
5. Arunkumar, A. I., Srisailam, S., Kumar, T. K., Kathir, K. M., Chi, Y. H., Wang, H. M., Chang, G. G., Chiu, I., and Yu, C. (2002) Structure and stability of an acidic fibroblast growth factor from *Notophthalmus viridescens*, *J. Biol. Chem. 277*, 46424−46432.
6. Ibrahimi, O. A., Zhang, F., Hrstka, S. C., Mohammadi, M., and Linhardt, R. J. (2004) Kinetic model for FGF, FGFR, and proteoglycan signal transduction complex assembly, *Biochemistry 43*, 4724−4730.
7. Sher, I., Yeh, B. K., Mohammadi, M., Adir, N., and Ron, D. (2003) Structure-based mutational analyses in FGF7 identify new residues involved in specific interaction with FGFR2IIIb, *FEBS Lett. 552*, 150−154.
8. Robson-Dixon, N. D., and Garcia-Blanco, M. A. (2004) MAZ elements alter transcription elongation and silencing of the fibroblast growth factor receptor 2 exon IIIb, *J. Biol. Chem. 279*, 29075−29084.
9. Yeh, B. K., Igarashi, M., Eliseenkova, A. V., Plotnikov, A. N., Sher, I., Ron, D., Aaronson, S. A., and Mohammadi, M. (2003) Structural basis by which alternative splicing confers specificity in fibroblast growth factor receptors, *Proc. Natl. Acad. Sci. U.S.A. 100*, 2266−2271.
10. Olsen, S. K., Ibrahimi, O. A., Raucci, A., Zhang, F., Eliseenkova, A. V., Yayon, A., Basilico, C., Linhardt, R. J., Schlessinger, J., and Mohammadi, M. (2004) Insights into the molecular basis for fibroblast growth factor receptor autoinhibition and ligand-binding promiscuity, *Proc. Natl. Acad. Sci. U.S.A. 101*, 935−940.
11. Chellaiah, A., Yuan, W., Chellaiah, M., and Ornitz, D. M. (1999) Mapping ligand binding domains in chimeric fibroblast growth factor receptor molecules. Multiple regions determine ligand binding specificity, *J. Biol. Chem. 274*, 34785−34794.
12. Wang, F., McKeehan, K., Yu, C., and McKeehan, W. L. (2002) Fibroblast growth factor receptor 1 phosphotyrosine 766: Molecular target for prevention of progression of prostate tumors to malignancy, *Cancer Res. 62*, 1898−1903.

13. Hung, K. W., Kumar, T. K. S., Chi, Y. H., Chiu, I. M., and Yu, C. (2004) Molecular cloning, overexpression, and characterization of the ligand-binding D2 domain of fibroblast growth factor receptor, *Biochem. Biophys. Res. Commun. 317*, 253−258.
14. Plotnikov, A. N., Schlessinger, J., Hubbard, S. R., and Mohammadi, M. (1999) Structural basis for FGF receptor dimerization and activation, *Cell 98*, 641−650.
15. Yeh, B. K., Eliseenkova, A. V., Plotnikov, A. N., Green, D., Pinnell, J., Polat, T., Gritli-Linde, A., Linhardt, R. J., and Mohammadi, M. (2002) Structural basis for activation of fibroblast growth factor signaling by sucrose octasulfate, *Mol. Cell. Biol. 22*, 7184−7192.
16. Springer, B. A., Pantoliano, M. W., Barbera, F. A., Gunyuzlu, P. L., Thompson, L. D., Herblin, W. F., Rosenfeld, S. A., and Book, G. W. (1994) Identification and concerted function of two receptor binding surfaces on basic fibroblast growth factor required for mitogenesis, *J. Biol. Chem. 269*, 26879−26884.
17. Harmer, N. J., Ilag, L. L., Mulloy, B., Pellegrini, L., Robinson, C. V., and Blundell, T. L. (2004) Towards a resolution of the stoichiometry of the fibroblast growth factor (FGF)-FGF receptor-heparin complex, *J. Mol. Biol. 339*, 821−834.
18. Plotnikov, A. N., Hubbard, S. R., Schlessinger, J., and Mohammadi, M. (2000) Crystal structures of two FGF−FGFR complexes reveal the determinants of ligand−receptor specificity, *Cell 101*, 413−424.
19. Schlessinger, J., Plotnikov, A. N., Ibrahimi, O. A., Eliseenkova, A. V., Yeh, B. K., Yayon, A., Linhardt, R. J., and Mohammadi, M. (2000) Crystal structure of a ternary FGF−FGFR−heparin complex reveals a dual role for heparin in FGFR binding and dimerization, *Mol. Cell 6*, 743−750.
20. Stauber, D. J., DiGabriele, A. D., and Hendrickson, W. A. (2000) Structural interactions of fibroblast growth factor receptor with its ligands, *Proc. Natl. Acad. Sci. U.S.A. 97*, 49−54.
21. Pellegrini, L., Burke, D. F., von Delft, F., Mulloy, B., and Blundell, T. L. (2000) Crystal structure of fibroblast growth factor receptor ectodomain bound to ligand and heparin, *Nature 407*, 1029−1034.
22. Pellegrini, L. (2001) Role of heparan sulfate in fibroblast growth factor signalling: A structural view, *Curr. Opin. Struct. Biol. 11*, 629−634.
23. Sasisekharan, R., Ernst, S., and Venkataraman, G. (1997) On the regulation of fibroblast growth factor activity by heparin-like glycosaminoglycans, *Angiogenesis 1*, 45−54.
24. Ashikari-Hada, S., Habuchi, H., Kariya, Y., Itoh, N., Reddi, A. H., and Kimata, K. (2004) Characterization of growth factor-binding structures in heparin/heparan sulfate using an octasaccharide library, *J. Biol. Chem. 279*, 12346−12354.
25. Arunkumar, A. I., Kumar, T. K., Kathir, K. M., Srisailam, S., Wang, H. M., Leena, P. S., Chi, Y. H., Chen, H. C., Wu, C. H., Wu, R. T., Chang, G. G., Chiu, I. M., and Yu, C. (2002) Oligomerization of acidic fibroblast growth factor is not a prerequisite for its cell proliferation activity, *Protein Sci. 11*, 1050−1061.
26. Prakash, V., and Timasheff, S. N. (1985) Vincristine-induced self-association of calf brain tubulin, *Biochemistry 24*, 5004−5010.
27. Noe, V., Willems, J., Vandekerchlove, J., Roy, F. V., Bryoneel, E., and Mareel, M. (1999) Inhibition of adhesion and induction of epithelial cell invasion by HAV-containing E-cadherin-specific peptides, *J. Cell Sci. 112*, 127−135.
28. Hajduk, P. J., Meadows, R. P., and Fesik, S. W. (1999) NMR-based screening in drug discovery, *Q. Rev. Biophys. 32*, 211−240.
29. de Paz, J. L., Angulo, J., Lassaletta, J. M., Nieto, P. M., Redondo-Horcajo, M., Lozano, R. M., Gimenez-Gallego, G., and Martin-Lomas, M. (2001) The activation of fibroblast growth factors by heparin: Synthesis, structure, and biological activity of heparin-like oligosaccharides, *ChemBioChem 2*, 673−685.
30. Wu, Z. L., Zhang, L., Yabe, T., Kuberan, B., Beeler, D. L., Love, A., and Rosenberg, R. D. (2003) The involvement of heparan sulfate (HS) in FGF1/HS/FGFR1 signaling complex, *J. Biol. Chem. 278*, 17121−17129.
31. Roghani, M., Mansukhani, A., Dell'Era, P., Bellosta, P., Basilico, C., Rifkin, D. B., and Moscatelli, D. (1994) Heparin increases the affinity of basic fibroblast growth factor for its receptor but is not required for binding, *J. Biol. Chem. 269*, 3976−3984.
32. Delehedde, M., Seve, M., Sergeant, N., Wartelle, I., Lyon, M., Rudland, P. S., and Fernig, D. G. (2000) Fibroblast growth factor-2 stimulation of p42/44MAPK phosphorylation and IκB degradation is regulated by heparan sulfate/heparin in rat mammary fibroblasts, *J. Biol. Chem. 275*, 33905−33910.
33. Shireman, P. K., Xue, L., Maddox, E., Burgess, W. H., and Greisler, H. P. (2000) The S130K fibroblast growth factor-1 mutant induces heparin-independent proliferation and is resistant to thrombin degradation in fibrin glue, *J. Vasc. Surg. 31*, 382−390.
34. Brych, S. R., Dubey, V. K., Bienkiewicz, E., Lee, J., Logan, T. M., and Blaber, M. (2004) Symmetric primary and tertiary structure mutations within a symmetric superfold: A solution, not a constraint, to achieve a foldable polypeptide, *J. Mol. Biol. 344*, 769−780.
35. Turnbull, W. B., and Daranas, A. H. (2003) On the value of c: Can low affinity systems be studied by isothermal titration calorimetry? *J. Am. Chem. Soc. 125*, 14859−14866.
36. Zhang, T., and Johansson, J. S. (2003) An isothermal titration calorimetry study on the binding of four volatile general anesthetics to the hydrophobic core of a four-α-helix bundle protein, *Biophys. J. 85*, 3279−3285.
37. Pantoliano, M. W., Horlick, R. A., Springer, B. A., Van Dyk, D. E., Tobery, T., Wetmore, D. R., Lear, J. D., Nahapetian, A. T., Bradley, J. D., and Sisk, W. P. (1994) Multivalent ligand−receptor binding interactions in the fibroblast growth factor system produce a cooperative growth factor and heparin mechanism for receptor dimerization, *Biochemistry 33*, 10229−10248.
38. Chi, Y. H., Kumar, T. K. S., Kathir, K. M., Lin, D. H., Zhu, G., Chiu, I. M., and Yu, C. (2002) Investigation of the structural stability of the human acidic fibroblast growth factor by hydrogen−deuterium exchange, *Biochemistry 41*, 15350−15339.
39. Tugarinov, V., Hwang, P. M., and Kay, L. E. (2004) Nuclear magnetic resonance spectroscopy of high-molecular-weight proteins, *Annu. Rev. Biochem. 73*, 107−146.
40. Bax, A., and Grzesiek, S. (1993) Methodological advances in protein NMR, *Acc. Chem. Res. 26*, 130−138.
41. Cornilescu, G., Delaglio, F., and Bax, A. (1999) Protein backbone angle restraints from searching a database for chemical shift and sequence homology, *J. Biomol. NMR 13*, 289−302.
42. Markley, J. L., Bax, A., Arata, Y., Hilbers, C. W., Kaptein, R., Sykes, B. D., Wright, P. E., and Wuthrich, K. (1998) Recommendations for the presentation of NMR structures of proteins and nucleic acids: IUPAC−IUBMB−IUPAB Inter-Union Task Group on the standardization of data bases of protein and nucleic acid structures determined by NMR spectroscopy, *Eur. J. Biochem. 256*, 1−15.
43. Goddard, T. D., and Kneller, D. G. (2004) *SPARKY 3*, University of California, San Francisco.
44. Brunger, A. T., Adams, P. D., Clore, G. M., DeLano, W. L., Gros, P., Grosse-Kunstleve, R. W., Jiang, J. S., Kuszewski, J., Nilges, M., Pannu, N. S., Read, R. J., Rice, L. M., Simonson, T., and Warren, G. L. (1998) Crystallography & NMR system: A new software suite for macromolecular structure determination, *Acta Crystallogr. D54*, 905−921.
45. Laskowski, R. A., Moss, D. S., and Thornton, J. M. (1993) Main-chain bond lengths and bond angles in protein structures, *J. Mol. Biol. 231*, 1049−1067.
46. Korardi, R., Billeter, M., and Wuthrich, K. (1996) MOLMOL: A program for display and analysis of macromolecular structures, *J. Mol. Graphics 14*, 51−55.
47. Lerche, M. H., Meissner, A., Poulsen, F. M., and Sorensen, O. W. (1999) Pulse sequences for measurement of one-bond ^{15}N-^{1}H coupling constants in the protein backbone, *J. Magn. Reson. 140*, 259−263.
48. Farrow, N. A., Muhandiram, R., Singer, A. U., Pascal, S. M., Kay, C. M., Gish, G., Shoelson, S. E., Pawson, T., Forman-Kay, J. D., and Kay, L. E. (1994) Backbone dynamics of a free and phosphopeptide-complexed Src homology 2 domain studied by 15N NMR relaxation, *Biochemistry 33*, 5984−6003.

BI051030N